Progress In Electromagnetics Research C, Vol. 92, 113–121, 2019

Common-Mode Suppression in Broadside Coupled Coplanar Waveguides

Yujie He[1], Joseph M. Faia[1], Michael Cracraft[2], and Edward Wheeler[1, *]

Abstract—Differential signaling is used in digital circuitry and high speed communication links due to its lower level of radiation and lower susceptibility to interference. Signal skew, amplitude differences and unequal parasitic electric or magnetic coupling to nearby structures can lead to common-mode signals being present on differential communication links which can result in unwanted electromagnetic interference and crosstalk. Common-mode filtering is often employed to suppress common-mode signal propagation in order to mitigate against these negative effects. In this paper broadside coupled differential coplanar waveguides are used which provide effective differential transmission from *dc* through 40 GHz. Simulation and measurement show that dipole-like common-mode filtering elements placed between the broadside coupled traces offer common-mode suppression of more than 10 dB over bandwidths greater than 5 GHz. A design equation is developed which can be used to estimate filtering frequencies from filter dimensions through 30 GHz. Filters can be cascaded to broaden filtering around a single frequency to filter at multiple frequencies. Simulation based registration studies were conducted which show stable filtering performance in the presence of layer-to-layer misregistration up to 0.254 mm.

1. INTRODUCTION

Differential signaling is frequently used in digital circuitry and high speed communication links because of its lower level of radiation and its lower susceptibility to interference. In any practical differential signaling structure, signal skew, amplitude differences and unequal parasitic electric or magnetic coupling to nearby structures can lead to the presence of a common-mode (CM) signal which can, in turn, result in higher levels of electromagnetic interference (EMI) and crosstalk. CM filtering structures can be used in differential transmission lines to suppress common-mode signal propagation, thereby avoiding the negative effects of CM propagation.

Past work to suppress common-mode propagation in microstrip or stripline differential transmission lines has included patterned ground structures [1–5], electromagnetic bandgap structures [6–8], periodic structures [9], and metamaterial inspired structures such as complementary split-ring resonators [5, 10–13]. Less effort has been directed toward investigating common-mode suppression in differential coplanar waveguides. Table 1 lists transmission line type, filter design, center frequency, and fractional bandwidth for some of the previous work in common-mode filtering along with the results reported here.

In this paper, we investigate effective differential transmission and CM suppression in broadside coupled coplanar waveguides (BC CPWs) which comprise two conventional CPWs, one on top of the other, separated by a dielectric. Earlier work on coupled coplanar waveguides [14], Beldair and Wolff, assuming differential excitation, placed one reference conducting plane at the resulting electric wall shown in Figure 1(a) and added another above the CPW to produce the single-ended structure shown in Figure 1(b). For the resulting single-ended structure, they employed numerical analysis to reveal four limiting cases distinguished by geometry and permittivity.

Received 17 January 2019, Accepted 24 April 2019, Scheduled 25 April 2019
* Corresponding author: Edward Wheeler (wheeler@rose-hulman.edu).
[1] Department of Electrical and Computer Engineering, Rose-Hulman Institute of Technology, 5500 Wabash Ave., Terre Haute, IN 47803, USA. [2] IBM Systems and Technology Group, Poughkeepsie, NY 12603, USA.

Table 1. Results from current and past work in common-mode filtering.

Transmission line type	*Filter design*	*Center frequency*	*Fractional BW*
broadside-coupled CPW (results presented here)	$\lambda/2$ resonator	15 GHz (single filter) 16 GHz (cascade)	42.5% 61.5%
differential microstrip	defected ground structure (DGS)	6.35 GHz [1] 5.4 GHz [3]	87% 130%
	electromagnetic bandgap (EBG)	4.95 GHz [6] 14.25 GHz [7]	6.1% (est.) 17.5% (est.)
	periodic structures	8 GHz [9]	30% (est.)
	CSRR	1.5 GHz [10]	40% (est.)
	DS-CSRR	1.5 GHz [10]	43% (est.)
	OCSRR	0.9 GHz [11]	73% (est)
differential stripline	EBG structures	12.5 and 15.1 GHz [7]	21.4% (est.)

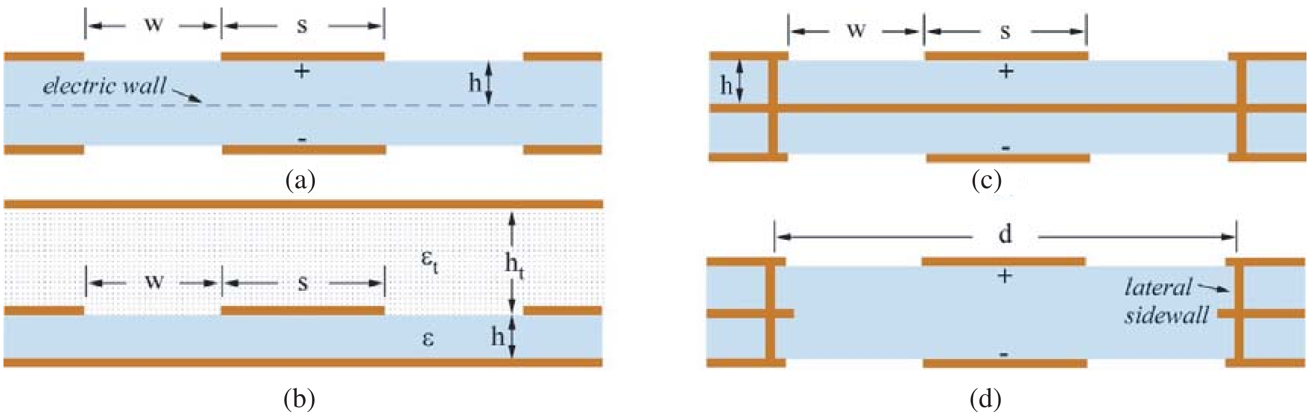

Figure 1. (a) Cross-section of the broadside coupled coplanar waveguide with a differential signal and (b) single-ended CPW with reference conductors above and at the electric wall, (c) cross-section of the BC CPW with lateral sidewalls and a conducting plane at the position of the electric wall and (d) cross-section with lateral sidewalls and no conducting plane.

The BC CPWs investigated here — with a relatively large slot width (w) together with no upper conducting plane (h_t large) — fall into the fourth case where the flux for a differential signal is largely between the trace and the lower conducting plane (or electric wall in the BC CPW). One therefore would expect little change in the flux structure under differential excitation if a third layer of metallization were placed at the electric wall as shown in Figure 1(c). There would likewise be little variation in the electric flux pattern as the cross-section alternates from that shown in Figure 1(c) to that shown in Figure 1(d) and vice versa.

Even though the presence of the lateral sidewalls cannot be ignored since d is not greater than 8 h [15], the dominant flux for Figure 1(c) is between the traces and the reference layer between them and between the traces for Figure 1(d). This is illustrated in the flux plots in Figures 2(a) and 2(b), which were obtained employing CST Microwave Studio (MWS).

Contrast this with CM excitation applied to the BC CPW shown in Figures 1(c) and 1(d) as illustrated in Figures 2(c) and 2(d). Effective differential-mode (DM) transmission together with CM suppression might therefore be expected since placing a reference plane between the two CPWs alters common-mode flux patterns significantly while altering differential pattern to a much lesser degree.

Equally important here is the fact that the middle metallization layer receives net flux when a CM signal is present (Figure 2(c)) with no net flux from a DM signal (Figure 2(a)). The net flux from

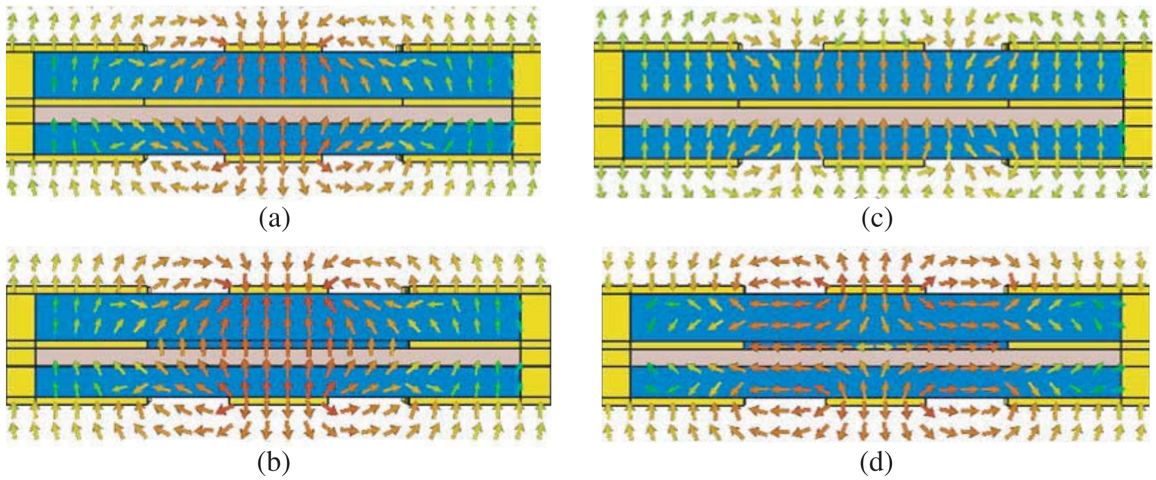

Figure 2. All plots obtained using CST MWS, (a) DM flux with conducting reference plane between the traces, (b) DM flux with no reference plane present, (c) CM flux with conducting reference plane between the traces, (d) CM flux with no reference plane present.

a CM signal allows half-wavelength dipole resonant structures in the middle metallization layer to be employed for CM suppression while the absence of net flux from DM signal prevents resonance to allow effective DM transmission. One can enumerate desirable attributes for the BC CPW structure to be useful as a differential communication link. These include i) DM transmission with low attenuation and dispersion, ii) CM filters offering suppression over a wide frequency range, iii) design equations allowing designers to estimate filtering frequencies, iv) relative robust performance in the presence of layer misregistration and v) effective launch structures allowing contacts to be made from one side of the printed circuit board (PCB). In this paper, modeling, simulation, and measurement are used to demonstrate the first four attributes with the fifth pertaining to signal launches from one side of the board remaining for future work.

2. BOARD STACKUP AND FILTER DESIGN

BC CPW waveguides comprising two single-ended CPWs, with vias connecting reference layers to provide lateral sidewalls, are the differential transmission lines used in this investigation. The CM filtering elements considered here are dipole-like resonant structures placed in the middle metallization layer.

Simulation and measurement results demonstrate that this differential transmission line offers CM suppression over wide bandwidths with effective DM transmission from *dc* to 40 GHz.

Rogers RO4350B laminates ($\varepsilon_r = 3.48$ and a loss tangent of 0.0037 at 10 GHz) with bonding by Rogers 4450F bondply ($\varepsilon_r = 3.52$ and a loss tangent of 0.004 at 10 GHz). These were also used in all CST MWS simulations. The lateral sidewall was realized through via fences placed along the CPW transmission line, which have the added benefit of preventing filtered CM energy from exciting parallel-plane waveguide modes [12]. In addition to the 3D modeling, 2D cross-sectional models were constructed. The stackup and dimensions of the printed circuit board (PCB) are shown in Figure 3. Details of the filtering layer (the middle layer of metallization in the stackup) are shown in Figure 4.

The filter behavior can be replicated with transmission line models from cross-sectional analysis. However, in its simplest form, this analysis neglects the effects of the connection between the filter element and the adjacent reference plane. Models are developed for the CM filtering elements, which allow the filtering frequencies to be predicted using a simple design equation for frequencies through 30 GHz.

The transmission line and filter structures may be represented as three- and four-line multiconductor transmission line structures, as in Figure 5(a). The unfiltered region comprises a three-line structure, two signal conductors, and three layers of reference metal approximated as a single conductor. Modeled

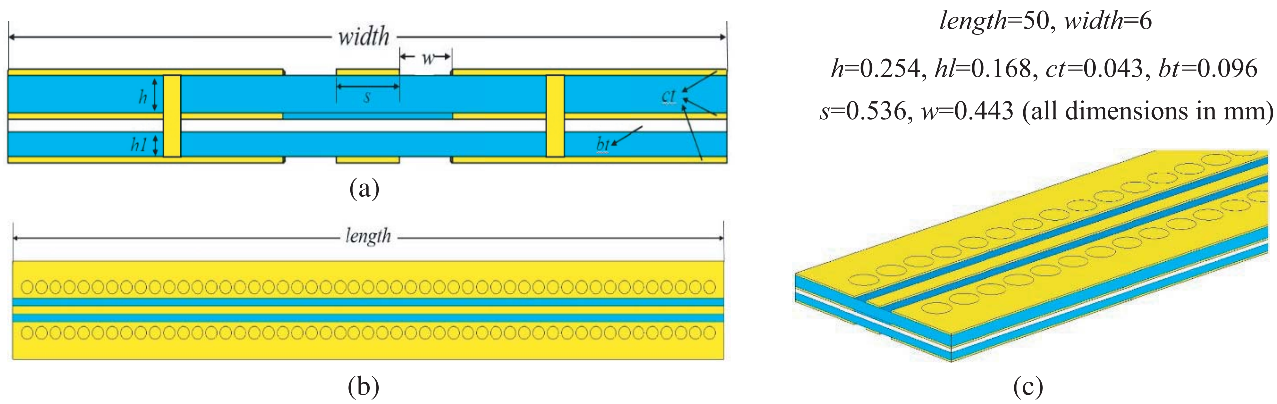

Figure 3. (a) Cross-section view of the PCB, bonding film shown in white, (b) top view, identical to the bottom view, (c) close-up perspective view.

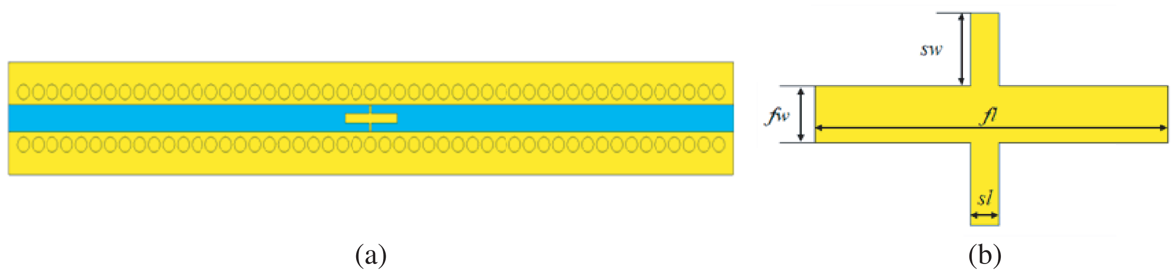

Figure 4. (a) Filter layer (middle layer metallization) and (b) Close-up view of a the filter structure.

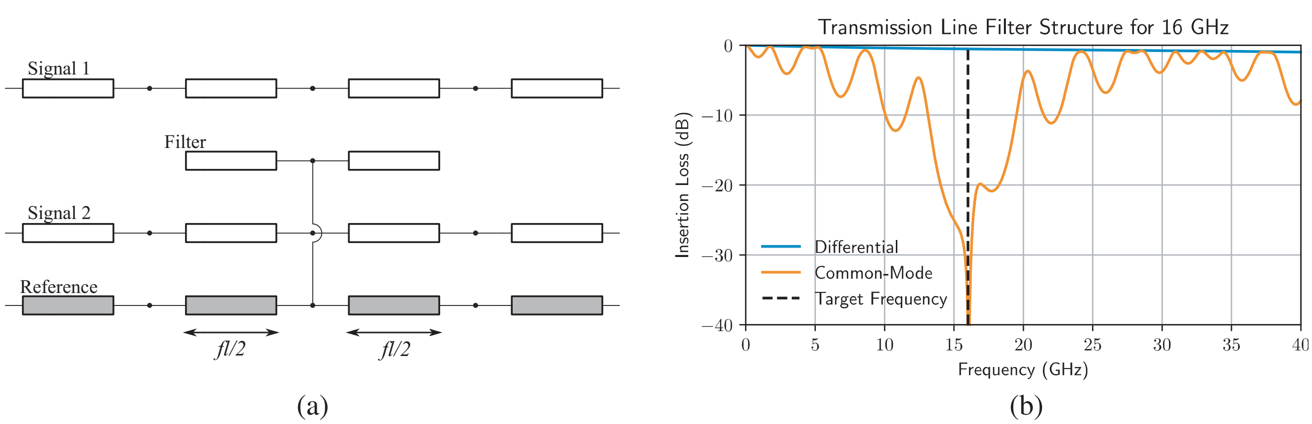

Figure 5. (a) Transmission line approximation with no parasitics, (b) differential and common-mode insertion loss responses for the transmission line model of the broadside coupled filter represented in Figure 5.

similar to Figure 3(a), the via wall is represented as a solid vertical connection between the reference planes, which helps justify treating the references as a single conductor in this simplified model. A fourth line was introduced to the model in the filtering region. The connection between center of the filter element and the reference was approximated a lumped short (no parasitics represented).

The filter structures resemble a shorted dipole, and these filters resonate similarly at odd multiples of a half wavelength. Through modal analysis not covered in the scope of this paper, the effective wavelength at 16 GHz in the four-line transmission line structure was found to be 10.06 mm, which leads to $fl = 5.03$ mm. The three-line structures stretch the rest of the 50 mm length.

Figure 5(b) shows the insertion loss for both modes. The differential is unperturbed while the common-mode experiences a large amount of loss over a wide band centered around 16 GHz.

For $fl \gg sw$, one can estimate the filtering frequency by taking fl as one-half wavelength at the desired CM filtering frequency. As fl decreases, sw and even fw amount to a significant amount of electrical length. Therefore, expression for fl must be amended to account for the electrical length of the shorting connection and the width of the filter patch itself.

$$\frac{l_{\text{eff}}}{2} = sw + \frac{fl}{2} + \frac{fw}{2} = n\frac{\lambda}{4} \quad n = 1, 3, \dots \tag{1}$$

The resulting design Equation (1) effectively estimates CM filtering frequencies for the PCB stackup employed here through 30 GHz, as will be demonstrated in Section 3. We have performed parameter sweeps to demonstrate that the differential CPW waveguide's transmission and CM filtering is maintained in the presence of moderate levels of layer-to-layer misregistration.

3. MEASUREMENT AND RESULTS

Measurements were carried out at two facilities on two different samples. At the first facility, shown in Figure 6(a), two 500 μm GGB RF probes are connected to an Agilent E8363B 40 GHz 2-port VNA through 2.92 mm cables. Additional GGB RF probes with 50 Ω broadband loads are connected to unused ports for each 2-port measurement with SOLT calibration performed at the end of the cables. Measurements conducted at the second facility, shown in Figure 6(b), employed an Agilent N5242A 4-port 26.5 GHz VNA with 2.92 mm cables and GGB RF probes. The same calibration technique is performed before measurements.

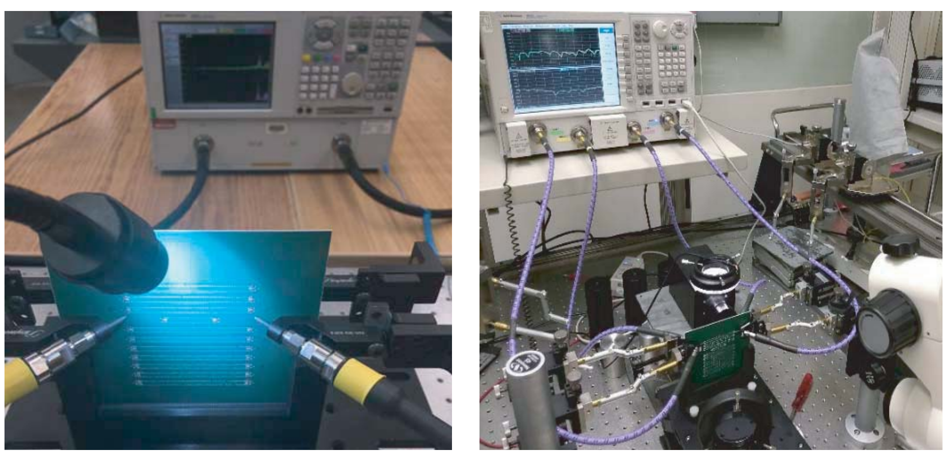

(a) (b)

Figure 6. (a) PCB measurement setup with a 2-port VNA. The broadband 50 Ω loads are on the other side of the test board, (b) PCB measurement setup with a 4-port VNA.

3.1. Filtering at a Single Frequency

A differential CPW structure with a single filtering structure as illustrated in Figure 5 was investigated first. The structure dimensions were designed for CM filtering at 16 GHz using design Equation (1). Measurement results are shown together with simulation in Figure 7. The simulated −10 dB bandwidth is 6.14 GHz and is centered at 15 GHz, demonstrating CM filtering over a broad band.

De-embedding using the auto fixture removal (AFR) technique is available for the 26.5 GHz measurements which are shown in Figure 7(a) [16, 17]. The de-embedded DM transmission is in good agreement with simulation showing effective DM transmission. The measured −10 dB bandwidth for CM filtering is 8.13 GHz which easily includes the 16 GHz target filtering frequency.

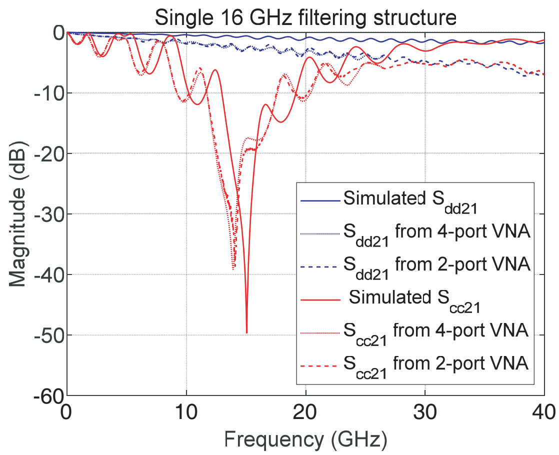

(a)

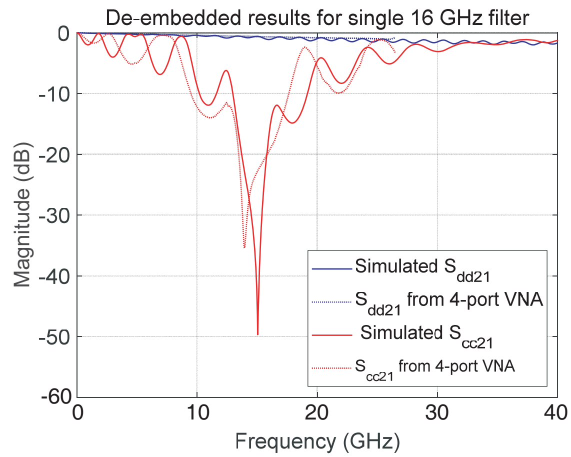

(b)

Figure 7. (a) Measured and simulated transmission DM and CM transmission for a differential CPW structure with a single 16 GHz filter, (b) de-embedded measured and simulated results for a single 16 GHz filter (note 0–26.5 GHz frequency range).

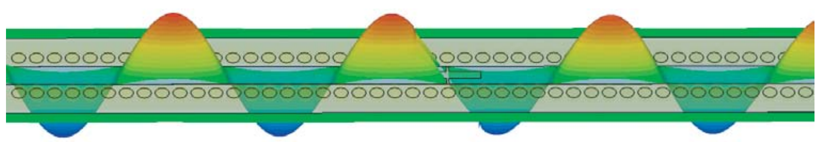

(a)

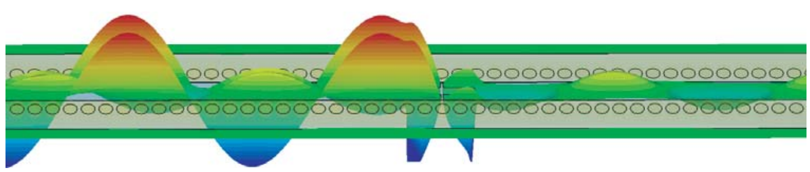

(b)

Figure 8. (a) Response showing effective transmission for a pure differential signal, (b) response showing the common-mode filtering.

Figure 8 illustrates field simulations of the waveguide with a common-mode filter present. Figure 8(a) shows the electric field when the 15 GHz signal is a pure differential signal, clearly showing effective propagation of the differential signal. Figure 8(b) shows the response the signal is pure common mode (note that S_{cc21} at 15 GHz is approximately -32 dB) showing the effectiveness of the common-mode filter.

3.2. Filtering at Multiple Frequencies

The filtering structures can be cascaded. Multiple filters of the same size can be cascaded to obtain deeper and broader filtering around the design frequency. If filtering at multiple frequencies is desired, filters of different sizes can be cascaded to achieve this goal. This is illustrated in Figures 9 and 10 with the filters shown in Figure 9 and the resulting filtering shown in Figure 10. The filter larger in size is designed to filter at the lower frequency, here 16 GHz, and the smaller filter designed to filter at 32 GHz.

Figure 10 shows simulation and measurement for the cascade filter with the simulation shown in Figure 10(a) using the process value for the relative permittivity of 3.48 (used in the CST material library for RO4350B laminate) and that shown in Figure 10(b) using the design value of 3.66. Effective DM transmission is shown for the cascade filter design with the filtering frequencies in simulation of 15.1 GHz and 30.5 GHz (Figure 10(a)) and 14.75 GHz and 29.85 GHz (Figure 10(b)) in simulation. Compared

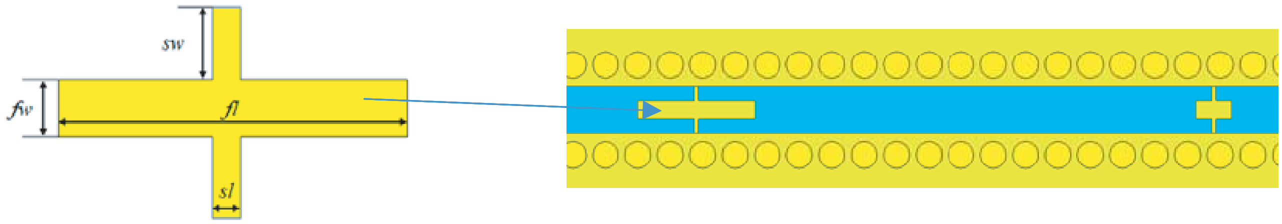

Figure 9. Cascade of two filtering structures, the larger (highlighted) designed for 16 GHz and the smaller designed for 32 GHz. Dimensions for 16 GHz filter (in mm): $fl = 3.698$, $fw = 0.536$, $sw = 0.443$, $sl = 0.125$. Dimensions for 32 GHz filter (in mm): $fl = 1.090$, $fw = 0.536$, $sw = 0.443$, $sl = 0.125$ mm.

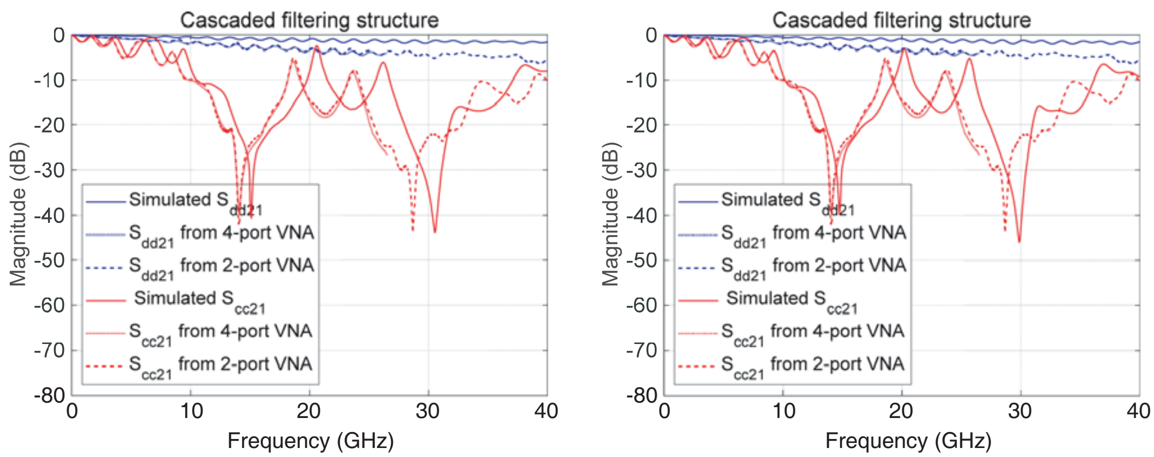

(a) (b)

Figure 10. Measured and simulated transmission results for cascaded 16 and 32 GHz filter structure, (a) used in simulation and (b) $\varepsilon_r = 3.66$ used (obtained by Rogers through averaging over several lots of laminate material).

with each is the measured filtering frequencies of 14.07 GHz and 28.64 GHz with 10 dB bandwidths of 8.175 GHz and 14.61 GHz, respectively.

3.3. Registration Study

In multilayer PCB fabrication processes, robust performance in the presence of moderate layer-to-layer misregistration is important if one is to avoid system performance being compromised by manufacturing tolerances. Previous researchers observed that misregistration can be a significant source of DM to CM conversion [18]. The parameter sweeps illustrated in Figure 12 demonstrate the differential CPW waveguide's transmission, and CM filtering is maintained in the presence of moderate levels of layer-to-layer misregistration.

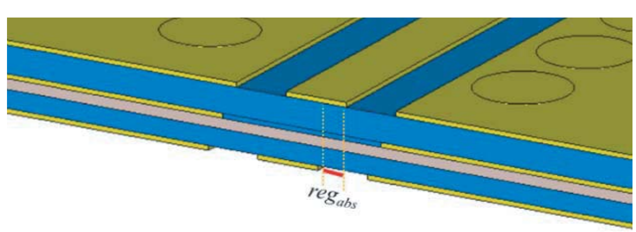

Figure 11. Side view with the trace-to-trace misregistration, reg_{abs}, labeled.

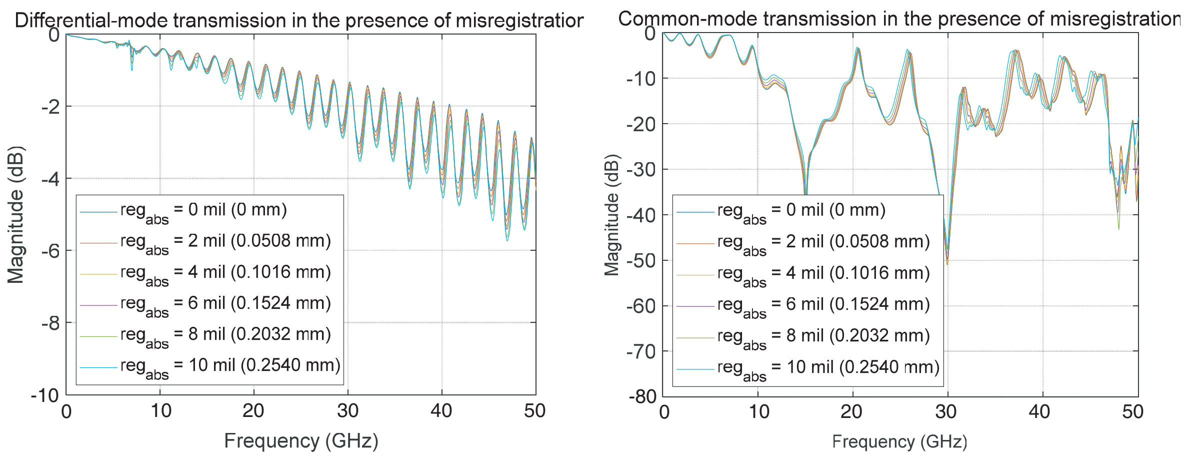

(a) (b)

Figure 12. Simulated results of the registration study: (a) differential mode signal transmission; (b) common mode signal transmission.

The distance from the center of the transmission line to the vertical center axis of the board (*reg*) was swept from 0 to 5 mils. In each simulation, the top and bottom signal lines move this distance from the center in opposite directions so that the trace-to-trace misregistration, as illustrated in Figure 11 and denoted as reg_{abs}, is twice the value of *reg* shown in Figure 11. The plots in Figure 12 show that these designs maintain robust performance in the presence of moderate misregistration, here demonstrated to 10 mils or 0.254 mm.

4. CONCLUSIONS

In this paper modeling, simulation, and measurement have been employed in an investigation of CM filtering in BC CPW structures. Results indicate that BC CPW with dipole-like resonant structures placed in the metallization layer between the traces offers effective DM transmission from *dc* through 40 GHz and at least 10 dB in CM attenuation over bandwidths greater than 5 GHz. A design equation was developed for the synthesis of filter elements, and simplified transmission line models were included to illustrate the relationship to the structure's dimensions. The filtering elements can be cascaded to filter at multiple frequencies or to broaden the filtering bandwidths. Registration studies are provided in which simulations show stable filtering performance in the presence of layer-to-layer misregistration up to 0.254 mm.

Future work includes development of launch structures to permit signal launch from a single side of the board including multiple, closely spaced launches to allow the analysis of possible effects of cross-talk. A second interesting area of investigation would be to investigate BC CPWs with smaller geometries since previous work with single-ended CPWs with lateral sidewalls demonstrated effective transmission to 500 GHz [19].

REFERENCES

1. Wu, S.-J., C.-H. Tsai, T.-L. Wu, and T. Itoh, "A novel wideband common-mode suppression filter for gigahertz differential signals using coupled patterned ground structure," *IEEE Trans. Microw. Theory Techn.*, Vol. 57, 848–855, Apr. 2009.
2. Liu, W.-T., C.-H. Tsai, T.-W. Han, and T.-L. Wu, "An embedded common-mode suppression filter for GHz differential signals using periodic defect ground plane," *IEEE Microw. Wireless Compon. Lett.*, Vol. 18, 248–250, May 2008.
3. Weng, T.-W., C.-H. Tsai, C.-H. Chen, D.-H. Han, and T.-L. Wu, "Synthesis model and design of a Common-Mode Bandstop Filter (CM-BSF) with an all-pass characteristic for high-speed differential signals," *IEEE Trans. Microw. Theory Techn.*, Vol. 62, 1647–1656, Aug. 2014.

4. Liu, Q., G. Li, V. Khilkevich, and D. Pommerenke, "Common-mode filters with interdigital fingers for harmonics suppression and lossy materials for broadband suppression," *IEEE Trans. Electromagn. Compat.*, Vol. 57, 1740–1743, Dec. 2015.
5. Martín, F., J. Naqui, A. Fernández-Prieto, P. Vélez, J. Bonache, J. Martel, and F. Medina, "The beauty of symmetry," *IEEE Microw. Mag.*, 42–55, Jan./Feb. 2017.
6. De Paulis, F., L. Raimondo, S. Connor, B. Archambeault, and A. Orlandi, "Design of a common-mode filter by using planar electromagnetic bandgap structures," *IEEE Trans. Adv. Packag.*, Vol. 33, 994–1002, Nov. 2010.
7. De Paulis, F., M. Cracraft, D. Di Febo, M. H. Nisanci, S. Connor, B. Archambeault, and A. Orlandi, "EBG-based common-mode microstrip and stripline filter design: Experimental investigation of performances and crosstalk," *IEEE Trans. Electromagn. Compat.*, Vol. 57, 996–1004, Oct. 2015.
8. Kodama, C., C. O'Daniel, J. Cook, F. de Paulis, M. Cracraft, S. Connor, A. Orlandi, and E. Wheeler, "Mitigating the threat of crosstalk and unwanted radiation when using electromagnetic bandgap structures to suppress common mode signal propagation in PCB differential interconnects," *Proc. IEEE Int. Symp. Electromagn. Compat.*, 622–627, Dresden, Germany, Aug. 2015.
9. Cracraft, M. and S. Connor, "Mode-selective periodic transmission line filters to reduce radiated common-mode emissions," *Proc. IEEE Int. Symp. Electromagn. Compat.*, 216–221, Ottawa, Canada, Jul. 2016.
10. Naqui, J., A. Fernández-Prieto, M. Durán-Sindreu, F. Mesa, J. Martel, F. Medina, and F. Martín, "Common-mode suppression in microstrip differential lines by means of complementary split ring resonators: Theory and applications," *IEEE Trans. Microw. Theory Techn.*, Vol. 60, 3023–3034, Oct. 2012.
11. Velez, P., J. Naqui, A. Fernández-Prieto, M. Durán-Sindreu, J. Bonache, J. Martel, F. Medina, and F. Martín, "Differential bandpass filter with commo-mode suppression based on open split ring resonators and open complementary split ring resonators," *IEEE Microw. Wireless Compon. Lett.*, Vol. 23, 22–24, Jan. 2013.
12. Sawyer, E., C. Kodama, C. O'Daniel, J. Cook, and E. Wheeler, "Using common-mode filtering structures with microstrip differential lines in a multilayer printed circuit board environment," *IEEE European Microw. Conf.*, 1091–1094, Rome, Italy, Oct. 2014.
13. He, Y., Z. Silva, Z. Bergstedt, J. Faia, S. Van Hoosier, S. G. Kang, G. Shaffer, E. Wheeler, and M. Cracraft, "Common-mode filtering in multilayer printed circuit boards," *Proc. IEEE Int. Symp. Electromagn. Compat.*, 288–292, Washington, DC, USA, Aug. 2017.
14. Bedair, S. S. and I. Wolff, "Fast and accurate analytic formulas for calculating the parameters of a general broadside-coupled coplanar waveguide for (M)MIC applications," *IEEE Trans. Microwave Theory Tech.*, Vol. 37, 843–850, May 1989.
15. Kretch, B. and R. Collin, "Microstrip dispersion including anisotropic substrates," *IEEE Trans. Microwave Theory Tech.*, Vol. 35, 710–718, Aug. 1987.
16. Keysight Technologies, Santa Rosa, CA, USA. Auto Fixture Removal (AFR), (2015) [Online], Available: http://na.support.keysight.com/plts/help/WebHelp/VNACalAndMeas/Auto_Fixture_Removal.htm, Accessed on: Apr. 20, 2018.
17. Keysight Technologies, Santa Rosa, CA, USA. Auto Fixture Removal (AFR), (2014) [Online], Available: http://na.support.keysight.com/vna/help/latest/S3_Cals/Auto_Fixture_Removal.htm, Accessed on: Apr. 20, 2018.
18. Shan, L., Y. Kwark, C. Baks, and M. Ritter, "Layer misregistration in PCB and its effects on signal propagation," *Proc. Electronic Components and Techn. Conf.*, 605–611, Las Vegas, NV, USA, Jun. 2010.
19. Fesharaki, F., T. Djerafi, M. Chaker, and K. Wu, "Low-loss and low-dispersion transmission line over DC-to-THz spectrum," *IEEE Trans. on Terahertz Science and Tech.*, Vol. 6, 611–618, Jul. 2016.